Supplementary: Extension, Development and Evaluation of the representation of the OH-initiated DMS oxidation mechanism in the MCM v3.3.1 framework

Lorrie S.D. Jacob[1], Chiara Giorio[1], and Alexander T. Archibald[1,2]

[1]Yusuf Hamied Department of Chemistry, University of Cambridge, Cambridge, CB2 1EW, UK
[2]National Centre for Atmospheric Science, Cambridge, CB2 1EW, UK

Correspondence: Lorrie S.D. Jacob (lj384@cam.ac.uk), Alexander T. Archibald (ata27@cam.ac.uk)

S1 Reactions added and adjusted from the MCM in the Jernigan, Shen and Ye mechanisms

The following tables provide the additions and adjustments to the MCM v3.3.1 DMS mechanism to make the Jernigan, Shen and Ye mechanisms (Jernigan et al., 2022; Shen et al., 2022; Ye et al., 2022) used in this work. The references for each of the reactions come directly from the papers themselves, and only changes to the sulfur reactions presented in the papers were included in these mechanisms. The 'adjusted' reactions refer to adjustments of rate constants or products of the reactions in the MCM.

Table S1: The reactions added to the base MCM mechanism to make the Ye et al. (2022) mechanism

	Reaction			Rate constant	Source
1	$CH_3SCH_2O_2$	=	$HOOCH_2SCH_2O_2$	9.00×10^{-2}	Ye et al. (2021)
2	$HOOCH_2SCH_2O_2$	=	HPMTF + OH	$5.8 \times 10^{11} \times e^{-10155/T+1080200/T^2}$	Wu et al. (2015)
3	$HOOCH_2SCH_2O_2$ + NO	=	$HOOCH_2SCH_2O$ + NO_2	$4.9 \times 10^{-12} \times e^{260/T}$	MCM v3.3.1 (SAR)
4	$HOOCH_2SCH_2O_2$ + HO_2	=	$HOOCH_2SCH_2OOH$	$1.13 \times 10^{-13} \times e^{1300/T}$	MCM v3.3.1 (SAR)
5	$HOOCH_2SCH_2O$	=	$HOOCH_2S$ + HCHO	1×10^{6}	MCM v3.3.1 (SAR)
6	HPMTF + OH	=	$HOOCH_2SCO$	1×10^{-11}	Vermeuel et al. (2020)
7	$HOOCH_2SCO$	=	$HOOCH_2S$ + CO	$9.2 \times 10^{9} \times e^{-505.4/T}$	Wu et al. (2015)
8	$HOOCH_2SCO$	=	OH + HCHO + OCS	$1.6 \times 10^{7} \times e^{-1468.6/T}$	Wu et al. (2015)
9	$HOOCH_2S$ + NO_2	=	$HOOCH_2SO$ + NO	$6.0 \times 10^{-11} \times e^{240/T}$	MCM v3.3.1 (SAR)
10	$HOOCH_2S$ + O_3	=	$HOOCH_2SO$	$1.15 \times 10^{-12} \times e^{430/T}$	MCM v3.3.1 (SAR)
11	$HOOCH_2SO$ + O_3	=	SO_2 + HCHO + OH	4.0×10^{-13}	MCM v3.3.1 (SAR)
12	$HOOCH_2SO$ + NO_2	=	SO_2 + HCHO + OH + NO	1.2×10^{-11}	MCM v3.3.1 (SAR)

Table S2: The reactions added to the base MCM mechanism in the Jernigan et al. (2022) mechanism. These reactions and their rate constants were taken from the equation and README files included in the archive containing the data for their paper.

	Reaction			Rate constant	Source
1	$CH_3SCH_2O_2$	=	HPMTF + OH	1.00×10^{-1}	Jernigan et al. (2022)
2	HPMTF + OH	=	OCS	$1.4 \times 10^{-11} \times 0.14$	Jernigan et al. (2022)
3	HPMTF + OH	=	SO_2 + CO	$1.4 \times 10^{-11} \times 0.86$	Jernigan et al. (2022)
4	OCS + OH	=	SO_2	$1.1 \times 10^{-13} \times e^{-1200/\mathrm{T}}$	Atkinson et al. (2004)
5	DMSO + OH	=	DMSO2	$6.10 \times 10^{-12} \times e^{800/\mathrm{T}} \times 0.1$	MCM v3.3.1 with Jernigan et al. (2022) branching ratio

Table S3: The reactions adjusted from the base MCM mechanism in the Jernigan et al. (2022) mechanism. These reactions and their rate constants were taken from the equation and README files included in the archive containing the data for their paper.

	Reaction			Rate constant	Source
1	$CH_3SCH_2O_2$	=	CH_3SCH_2O	$10 \times 10^{-12} \times [RO_2] \times 0.8$	based off Burkholder et al. (2019) self-reaction
2	$CH_3SCH_2O_2$	=	CH_3SCH_2OH	$10 \times 10^{-12} \times [RO_2] \times 0.1$	based off Burkholder et al. (2019) self-reaction
3	$CH_3SCH_2O_2$	=	CH_3SCHO	$10 \times 10^{-12} \times [RO_2] \times 0.1$	based off Burkholder et al. (2019) self-reaction
4	DMSO + OH	=	MSIA + CH_3O_2	$6.10 \times 10^{-12} \times e^{800/\mathrm{T}} \times 0.9$	MCM v3.3.1 with Jernigan et al. (2022) branching ratio

Table S4: The reactions added to the base MCM mechanism in the Shen et al. (2022) mechanism.

	Reaction			Rate constant	Source
1	$CH_3S(OH)CH_3$	=	DMS + OH	K_f/K_eq	Lucas and Prinn (2002)
2	$CH_3S(OH)CH_3$	=	HODMSO2	$8.5 \times 10^{-13} \times [O_2]$	Sander et al. (2011)
3	$CH_3S(OH)CH_3$	=	$CH_3SOH + CH_3O_2$	5.00×10^{5}	MCM v3.3.1
4	DMSO + OH	=	DMSO2	$6.10 \times 10^{-12} \times e^{800/T}/90$	Shen et al. (2022)
5	DMSO + NO_3	=	DMSO2 + NO_2	2.9×10^{-13}	Sander et al. (2011)
6	CH_3SOH + OH	=	CH_3SO	5.00×10^{-11}	MCM v3.3.1
7	MSIA + NO_3	=	$CH_3SO_2 + HNO_3$	1.00×10^{-13}	Yin et al. (1990)
8	$CH_3SOO + HO_2$	=	CH_3SOOH	4.00×10^{-12}	MCM v3.3.1
9	CH_3SOO	=	CH_3SO_2	1.00	Hoffmann et al. (2016)
10	CH_3SO_2 + OH	=	MSA	5.00×10^{-11}	Yin et al. (1990)
11	$CH_3SO_2 + NO_2$	=	$CH_3SO_3 + NO$	2.20×10^{-11}	Sander et al. (2011)
12	$CH_3SCH_2O_2$	=	$HOOCH_2SCH_2O_2$	HPTMF_isom	Veres et al. (2020); Berndt et al. (2019)
13	$HOOCH_2SCH_2O_2$	=	HPMTF + OH	HPTMF_isom2	Veres et al. (2020)
14	$HOOCH_2SCH_2O_2 + NO$	=	$HOOCH_2SCH_2O + NO_2$	$4.9 \times 10^{-12} \times e^{260/T}$	Wu et al. (2015)
15	$HOOCH_2SCH_2O$	=	$HOOCH_2S$ + HCHO	1.0×10^{6}	Wu et al. (2015)
16	$HOOCH_2SCH_2O_2 + HO_2$	=	$HOOCH_2SCH_2OOH$	$1.13 \times 10^{-13} \times e^{1300/T}$	Wu et al. (2015)
17	HPMTF + OH	=	$HOOCH_2SCO$	1.4×10^{-12}	Wu et al. (2015)
18	$HOOCH_2SCO$	=	$HOOCH_2S$ + CO	$9.2 \times 10^{9} \times e^{-505.4/T}$	Wu et al. (2015)
19	$HOOCH_2SCO$	=	OH + HCHO + OCS	$1.6 \times 10^{7} \times e^{-1468.6/T}$	Wu et al. (2015)
20	$HOOCH_2S + O_3$	=	$HOOCH_2SO$	$1.15 \times 10^{-12} \times e^{430/T}$	Wu et al. (2015)
21	$HOOCH_2S + NO_2$	=	$HOOCH_2SO + NO$	$6.0 \times 10^{-11} \times e^{240/T}$	Wu et al. (2015)
22	$HOOCH_2SO + O_3$	=	SO_2 + HCHO + OH	4.0×10^{-13}	Wu et al. (2015)
23	$HOOCH_2SO + NO_2$	=	SO_2 + HCHO + OH + NO	1.2×10^{-11}	Wu et al. (2015)
24	MSIA + O_3	=	MSA	2.00×10^{-18}	Lucas and Prinn (2002)
25	$CH_3SOH + O_3$	=	$CH_3O_2 + HO_2 + SO_2$	2.00×10^{-12}	Berndt et al. (2020)

Rate constants: K_f = $1.7 \times 10^{-42} \times [O_2] \times e^{7810/T} / (1 + 5.5 \times 10^{-31} \times [O_2] \times e^{7460/T})$, K_eq = $(8.3 \times 10^{-29} \times T \times e^{5136/T})$, HPTMF_isom1 = $2.2 \times 10^{11} \times e^{-9.8 \times 10^3/T} \times e^{1.0 \times 10^8/T^3} \times 5$, HPTMF_isom2 = $6.1 \times 10^{11} \times e^{-9.5 \times 10^3/T + 1.1 \times 10^8/T^3}$

Table S5: The reactions adjusted from the base MCM mechanism in the Shen et al. (2022) mechanism

	Reaction			Rate constant	Source
1	DMS + OH	=	$CH_3S(OH)CH_3$	$9.5 \times 10^{-39} \times [O_2] \times e^{5270/T} / (1 + 7.5 \times 10^{-29} \times [O_2] \times e^{5610/T})$	MCM v3.3.1
2	MSIA + OH	=	CH_3SO_2	1.60×10^{-11}	Yin et al. (1990)
3	$CH_3SO + O_3$	=	$CH_3O_2 + SO_2$	6.00×10^{-13}	Berndt et al. (2020)
4	CH_3SO_2	=	$CH_3O_2 + SO_2$	$8.80 \times 10^{14} \times e^{-9673/T}$	Wu et al. (2015)

S2 Modelling the Albu *et al.* experiment

As the Albu et al. (2008) experiment was not modelled in their paper, a different approach was taken to model their experiment. The input parameters for the model were taken from the experimental conditions described in the paper, however, the photolysis rate was not given and needed to be found through the best fit of the experimental data. In the case of Albu et al. (2008), ultraviolet (UV) lamps with a peak wavelength of 254 nm were used to photolyse the H_2O_2 in the reaction chamber into two OH radicals. The photolysis rate constant (J) of H_2O_2 was adjusted until a good fit was found with the loss of DMS measured in the experiment. The photolysis rate found to replicate the Albu et al. (2008) experiment was 1.4×10^{-4} s^{-1}, and the photolysis of products that absorbed at 254 nm (such as methyl hydroperoxide, CH_3OOH and methyl thioformate, MTF) were also included.

Figure S1 shows the loss of DMS observed by Albu et al. (2008) compared to the box model runs. The fit initially deviates from the experimental values. This deviation could be partly due to the experimental data being extracted from figures of Albu et al. (2008) using Webdigitizer. The digitisation of data can lead to some inconsistencies with the original data, such as the initial concentration not starting at the zeroth time step in Figure S1.

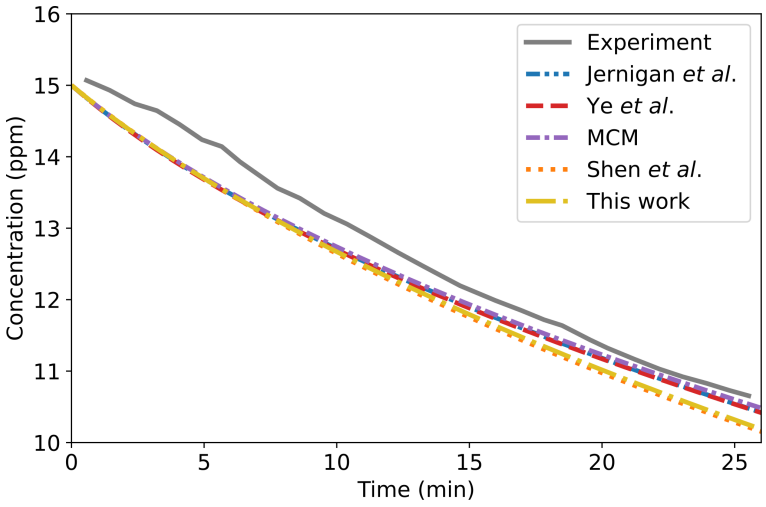

Figure S1. The measured DMS concentration in the Albu et al. (2008) experiment, compared to the model runs using different mechanisms (Jernigan, Ye, Shen, MCM, and the mechanism from this work). The photolysis rate of H_2O_2 was set so that the modelled loss of DMS matched the concentration measured.

S3 Modelling the Ye *et al.* experiment 1

The modelling of Ye et al. (2022) experiment 1 was initially replicated with the same input parameters as used in the paper, as shown in Figure 2 of the main text. However, for this study, one parameter was changed: the initial concentration of NO_2. In the modelling of experiment 1, the authors set the initial NO_2 concentration to zero, although it was measured to be 88 ppb at the start of the experiment. Figure S2 shows that changing the input NO_2 concentration to 88 ppb results in fewer OH radicals reacting with DMS in the model, which results in 35% less DMS reacting using the same mechanism used in the paper (Ye mechanism) and 41% less DMS reacted in the model compared to the experiment. The figure shows the raw DMS measured in the experiment, uncorrected for dilution, alongside the modelling from the Ye mechanism and the mechanism developed in this work (all of which include the loss of DMS from dilution). The pink dashed line represents the modelling conducted by Ye et al. (2022) in their paper, which was shown in Figure 2 of the main text. The red dashed line uses the same mechanism, however, includes the initial 88 ppb of NO_2; this modelling is used to represent the Ye mechanism in the rest of the paper.

The subsequent deviation between the model output and the measured loss of DMS is later explained as being due to the CH_3SO_3 radicals formed reacting with DMS to form methane sulfonic acid (MSA, CH_3SO_3H) and CH_3SCH_2, a reaction which was not included in the mechanism used by Ye et al. (2022) (this is discussed further in Section 5 of the main text). Our mechanism (yellow dot-dashed line), with the inclusion of this reaction, is able to replicate the measured DMS with the initial NO_2 concentration of 88 ppb.

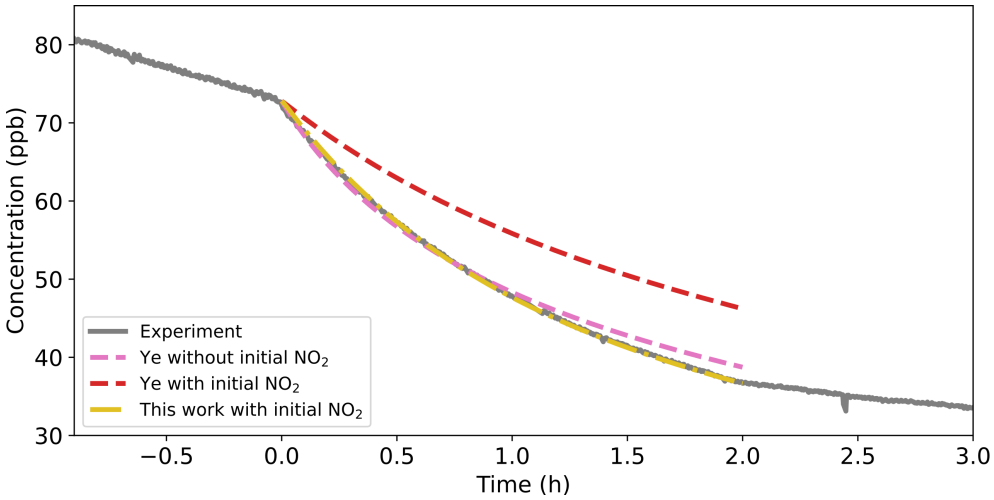

Figure S2. The raw measured DMS (grey solid line) from Ye et al. (2022) experiment 1, compared to the modelling of the Ye mechanism and the mechanism from this work (red dashed line and yellow dot-dashed line, respectively). In addition, the original modelling from Ye et al. (2022) is included (pink dashed line).

S4 Modelling of the different experiments

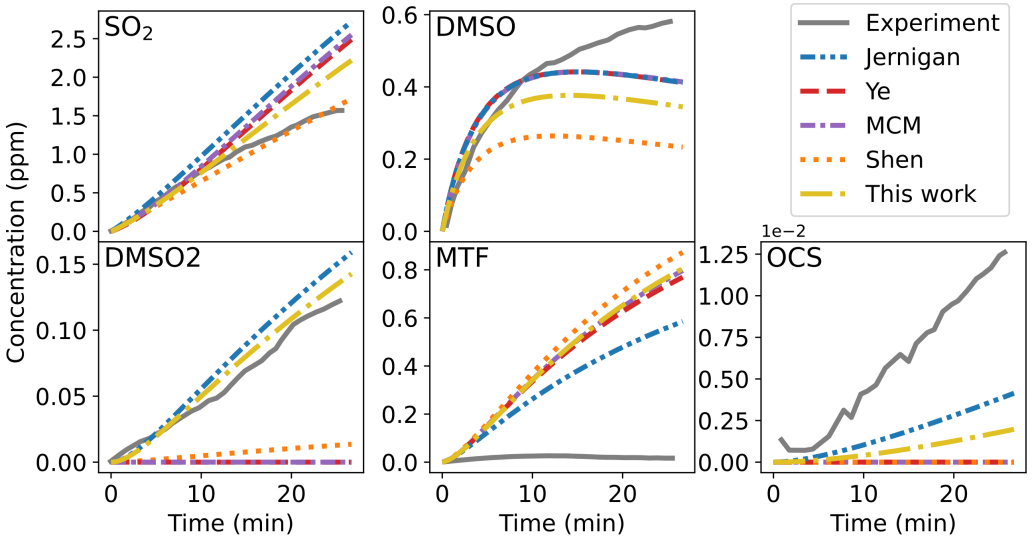

Figure S3. The products measured in the Albu et al. (2008) experiment, compared to the modelling results from the Jernigan, Ye, MCM and Shen mechanisms, along with the mechanism developed in this work.

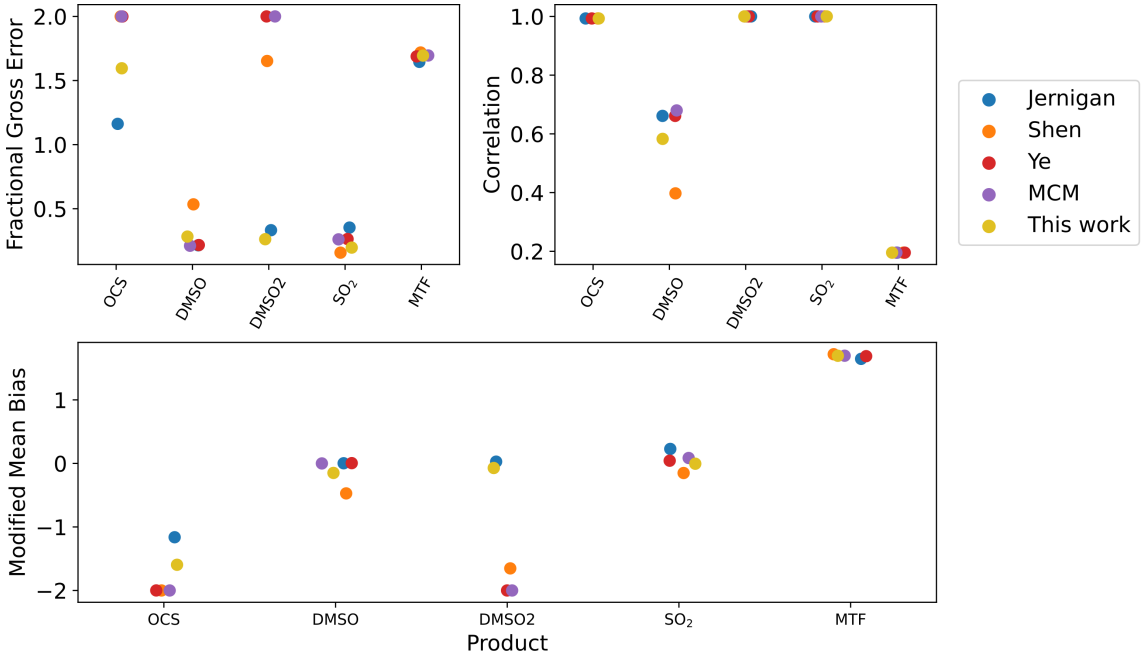

Figure S4. The fractional gross error, correlation coefficient and modified mean bias of the mechanisms for all species measured in the Albu et al. (2008) experiment.

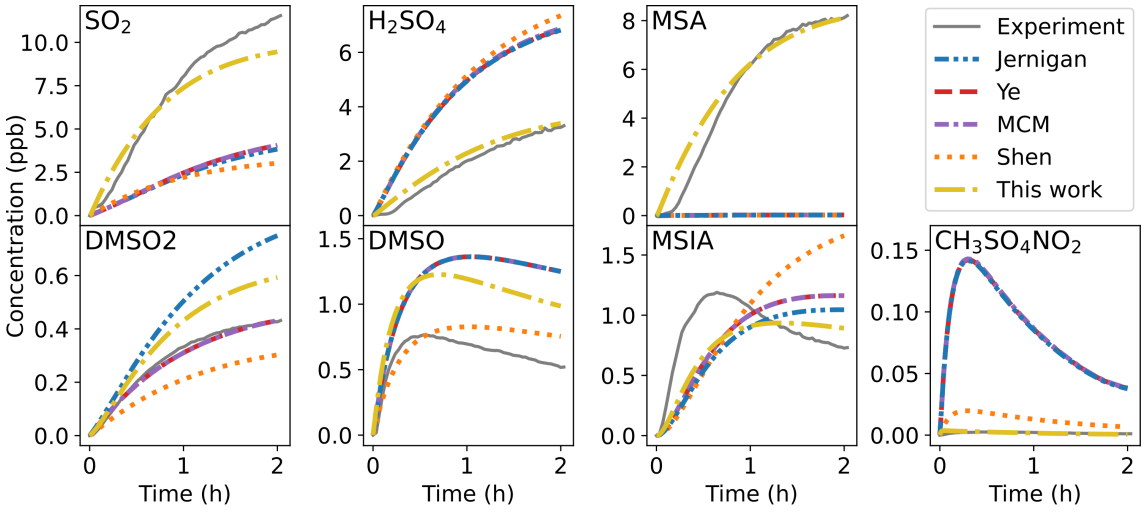

Figure S5. The products measured in the Ye et al. (2022) experiment 1, compared to the modelling results from the Jernigan, Ye, MCM and Shen mechanisms, along with the mechanism developed in this work. Note that the experimental DMSO2 represents the product $C_2H_6SO_2$ measured by Ye et al. (2022), which may also include CH_3SCH_2OOH.

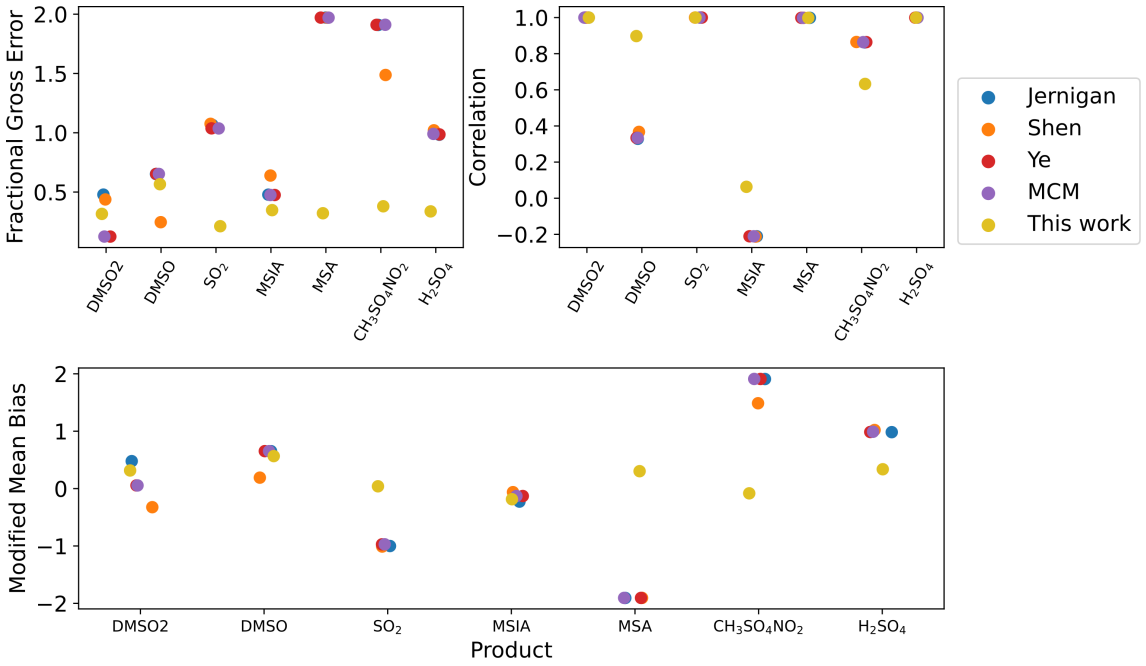

Figure S6. The fractional gross error, correlation coefficient and modified mean bias of the mechanisms for all species measured in the Ye et al. (2022) experiment 1. Note that the observed DMSO2 represents the product $C_2H_6SO_2$ measured by Ye et al. (2022), which may also include CH_3SCH_2OOH.

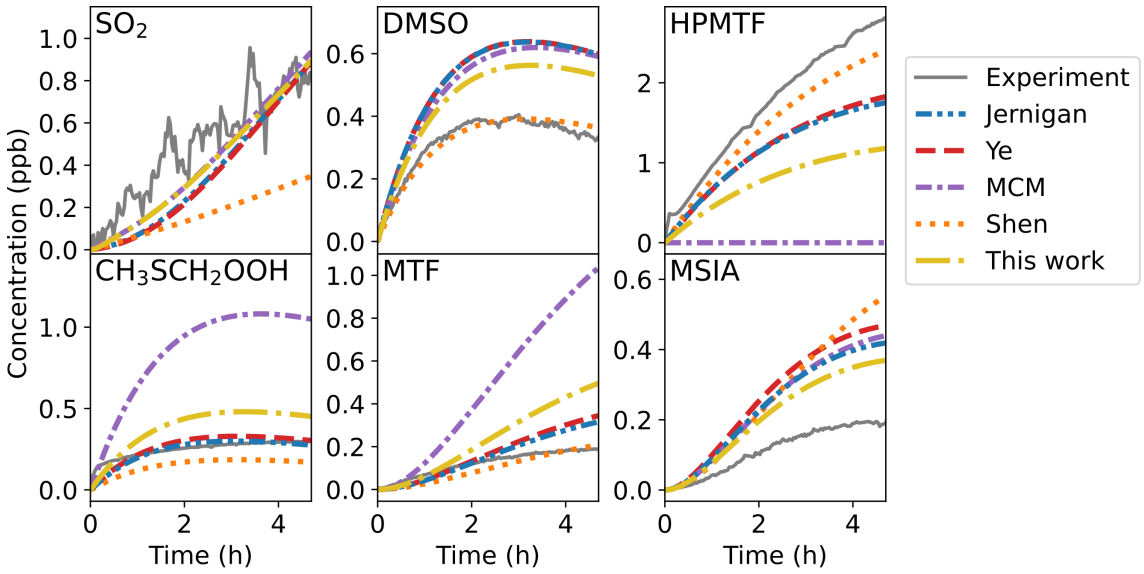

Figure S7. The products measured in the Ye et al. (2022) experiment 2a, compared to the modelling results from the Jernigan, Ye, MCM and Shen mechanisms, along with the mechanism developed in this work. Note that the experimental CH_3SCH_2OOH represents the product $C_2H_6SO_2$ measured by Ye et al. (2022), which may also include DMSO2.

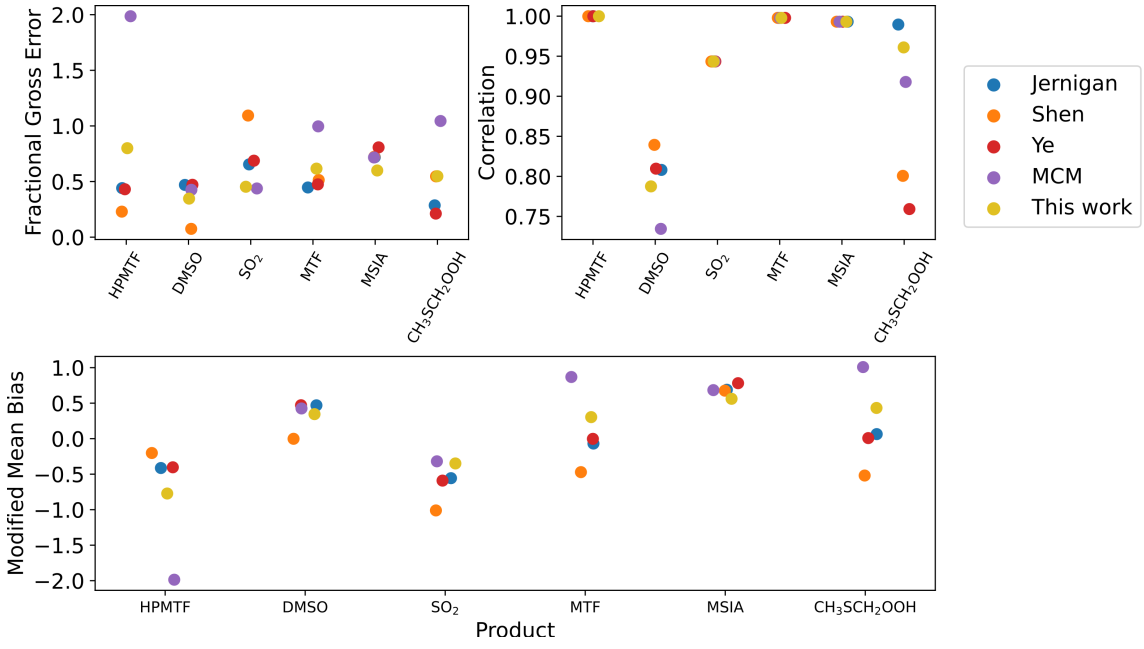

Figure S8. The fractional gross error, correlation coefficient and modified mean bias of the mechanisms for all species measured in the Ye et al. (2022) experiment 2a. Note that the observed CH_3SCH_2OOH represents the product $C_2H_6SO_2$ measured by Ye et al. (2022), which may also include DMSO2.

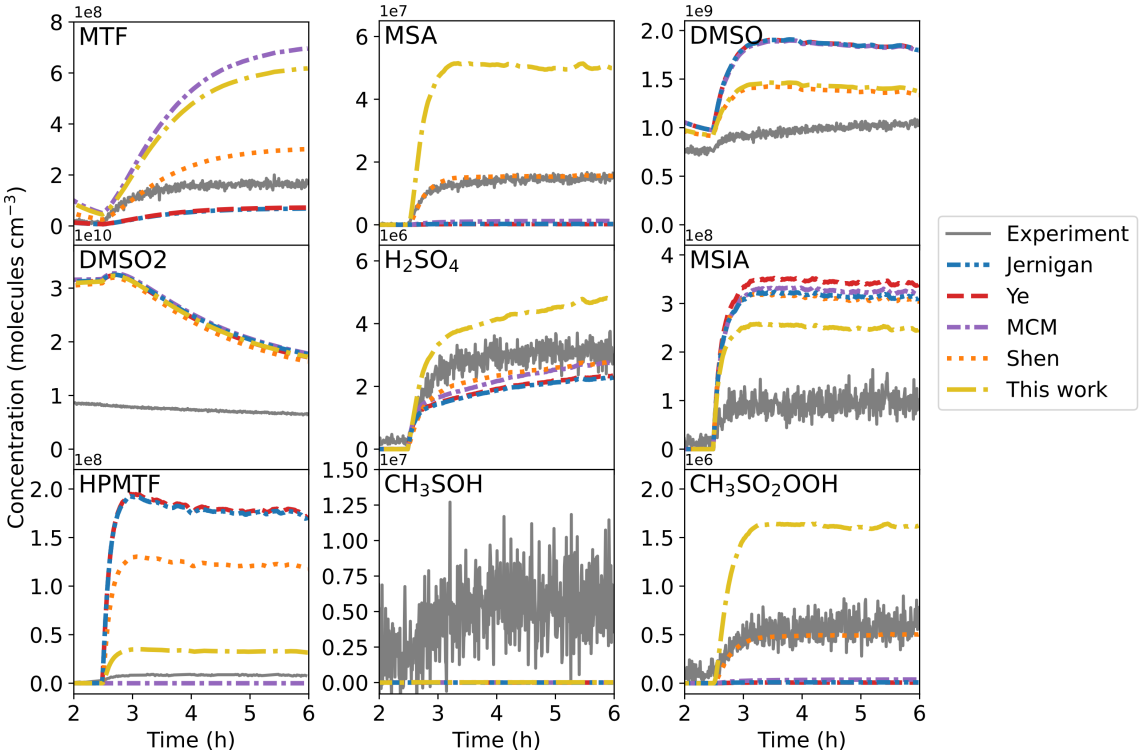

Figure S9. The products measured in the Shen et al. (2022) experiment, compared to the modelling results from the Jernigan, Ye, MCM and Shen mechanisms, along with the mechanism developed in this work.

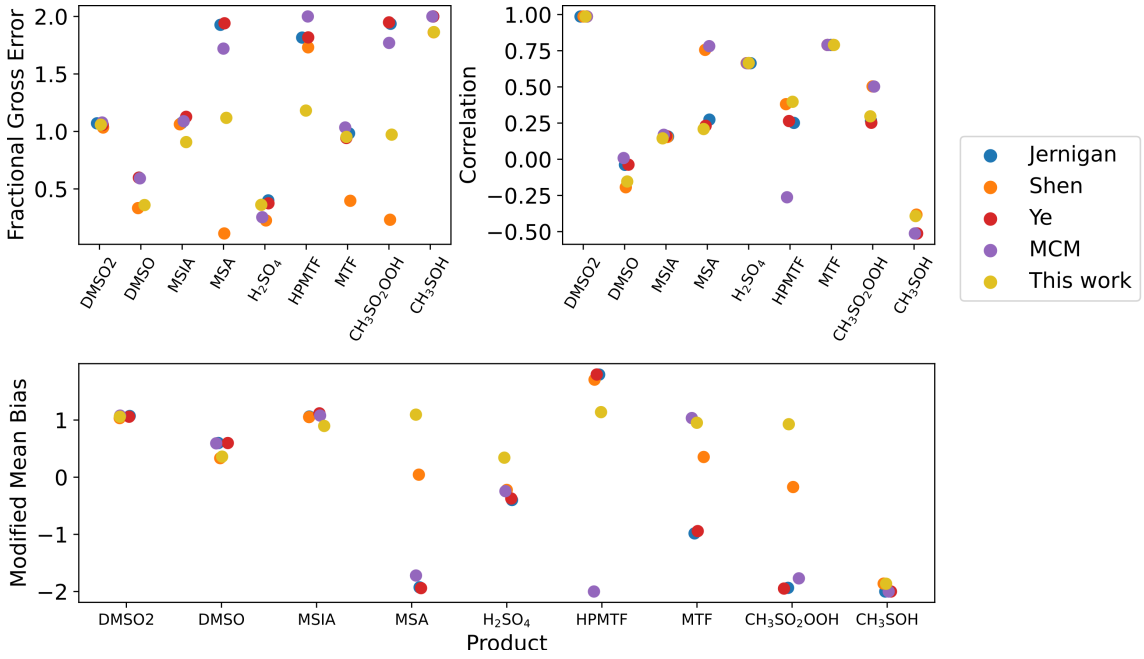

Figure S10. The fractional gross error, correlation coefficient and modified mean bias of the mechanisms for all species measured in the Shen et al. (2022) experiment.

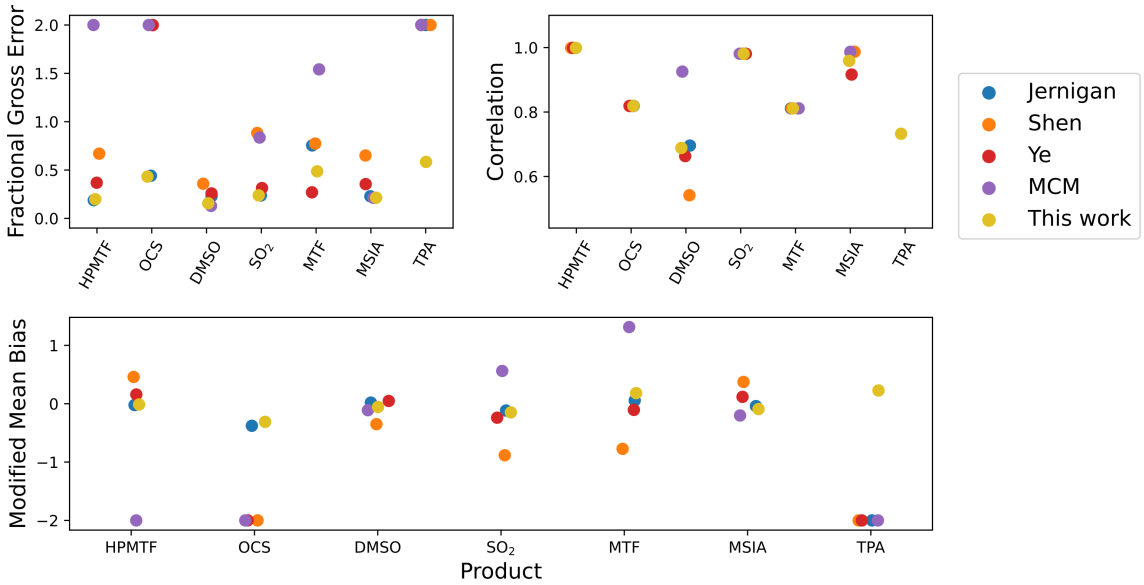

Figure S11. The fractional gross error, correlation coefficient and modified mean bias of the mechanisms for all species measured in the Jernigan et al. (2022) experiment.

S5 Modelling MSA in the Shen et al. (2022) experiment

Understanding the modelling of MSA in the Shen et al. (2022) experiment demonstrates the complexity of MSA formation, and allows an exploration of the uncertainties in the rate constants, and their temperature dependence (due to the experiment being conducted at 263 K). For that experiment, only the Shen mechanism and our mechanism modelled MSA with a fractional gross error of less than 1.5, although the MSA modelled through our mechanism is 3.6 times higher than measured (Figure S12). The MSA from all mechanisms came from the reaction of CH_3SO_3 with HO_2; the rate constant for that reaction is an estimate from Yin et al. (1990) and has not been measured experimentally. However, additional uncertainties arise when considering the modelling of CH_3SO_3 radicals.

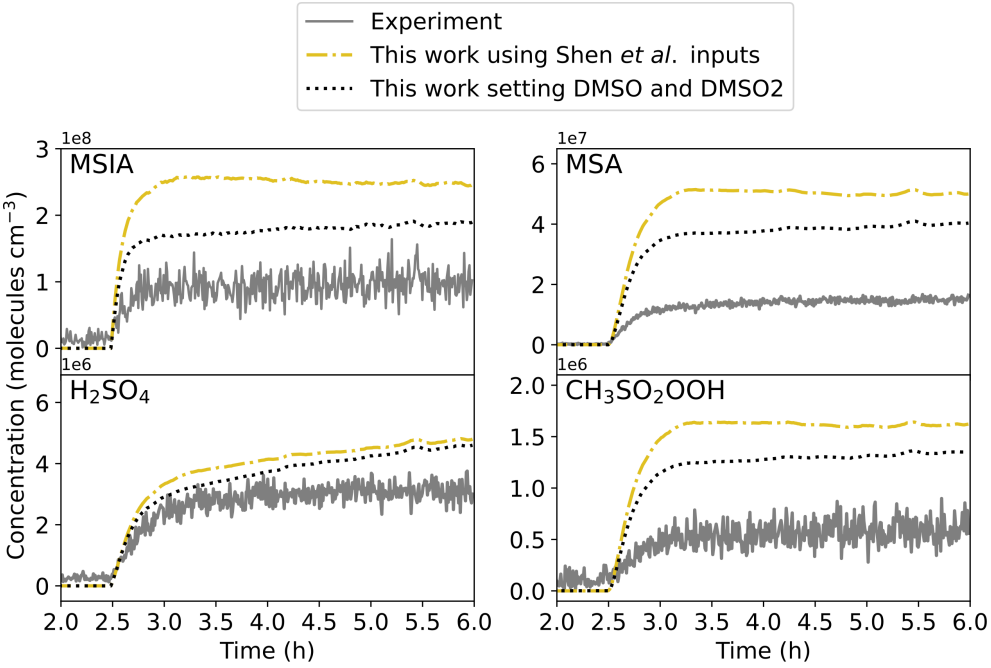

Figure S12. The measured MSIA, MSA, H_2SO_4 and CH_3SO_2OOH from the Shen et al. (2022) experiment (grey solid line), compared to the modelled results from the mechanism from this study, using the model inputs from the Shen et al. (2022) paper (yellow dot-dashed line), and from setting the DMSO and DMSO2 concentrations to those measured in the experiment (black dotted line).

In the Shen mechanism, and the mechanism developed in this study, the modelled CH_3SO_3 came from MSIA reacting with OH radicals; this reaction forms CH_3SO_2, which then typically dissociates to form SO_2 and CH_3 or eventually becomes the CH_3SO_3 radical (other pathways are possible, but minor). In the other mechanisms, the products of the MSIA reaction with OH are SO_2 and CH_3, which results in less MSA being produced by those mechanisms for this experiment (as no CH_3SO_3 forms through MSIA oxidation). There is only one study that measured the reaction between MSIA and OH, Kukui et al. (2003), which found that SO_2 formed at unit yield. However, that experiment was conducted in the absence of oxygen, which is needed to form CH_3SO_3, and products other than SO_2.

The mechanism from this work overestimates the MSA formed, which could be due to a few factors. As the MSIA modelled through our mechanism overestimates the experiments (2.6 times higher than measured), it could account for some of the overestimation of MSA in the model. The overestimation of MSA could also indicate that the rate constant used for the reaction between MSIA and OH (by Kukui et al. (2003)) is too fast at this temperature (263 K). Additionally, there are also large uncertainties in the reactions of CH_3SO_3 (including the reaction with HO_2 to form MSA), and the modelled concentration of HO_2.

The overestimation of MSIA from the models, formed from the reaction of DMSO with OH, can come from a few sources. The DMSO formed is also overestimated in the mechanisms, which would result in an overestimation of MSIA, however, DMSO (and DMSO2) formed in the Shen et al. (2022) experiment was found to come from both gas-phase reactions and wall reactions (which were included as part of the auxiliary mechanism). To investigate the formation of MSIA from DMSO, the DMSO and DMSO2 were set to the measured values (Figure S12, black dotted lines). Setting the DMSO to the measured values did decrease the MSIA modelled by 28%, however, the model still overestimated MSIA by around 89% compared to the measured MSIA concentration.

The rate constant for the DMSO and OH reaction forming MSIA is well established at 298 K (8.9×10^{-11} cm^3 $molecules^{-1}$ s^{-1}, Burkholder et al. (2019)), but only one temperature-dependent study was performed (at temperatures above room temperature) which contained large uncertainties. That study by Hynes and Wine (1996) found that the OH reaction with DMSO had a negative activation energy (the rate constant increased with decreasing temperature) where E/R = -800$\pm$540 K. However, to fit the MSIA formed, a rate constant slower than the rate constant determined at 298 K would be needed (5.7×10^{-11} cm^3 $molecules^{-1}$ s^{-1}). This indicates that the temperature dependence of this reaction should be studied further.

Further experiments on the reactions of DMSO and MSIA with OH radicals, and their temperature dependence, could improve the modelling of MSA at the lower temperatures studied in the Shen et al. (2022) experiments (263 K). Additionally, experiments to determine the rate of the reaction of CH_3SO_3 reaction with HO_2 could further improve MSA modelling in the marine environment.

S6 Marine boundary layer set up

Table S6. The initial and background concentrations of species used in the remote marine boundary layer run

Species	Concentration (ppm)
M	1×10^{6}
N_2	7.8×10^{5}
O_2	2.1×10^{5}
H_2O	1×10^{4}
CH_4	1.8
CO	0.1
H_2	0.5
O_3	3×10^{-2}
H_2O_2	1×10^{-3}
NO	1×10^{-6}
NO_2	1×10^{-5}
HNO_3	5×10^{-4}
DMS	2×10^{-4}
SO_2	2×10^{-5}

Table S7. The temperature and planetary boundary layer (PBL) height over the diurnal cycle.

Time (h)	Temperature (K)	PBL height (m)
0	289.5359	1300
1	289.1363	1300
2	289.0000	1350
3	289.1363	1400
4	289.5359	1450
5	290.1716	1500
6	291.0000	1550
7	291.9647	1450
8	293.0000	1400
9	294.0353	1350
10	295.0000	1300
11	295.8284	1250
12	296.4641	1200
13	296.8637	1200
14	297.0000	1200
15	296.8637	1200
16	296.4641	1150
17	295.8284	1150
18	295.0000	1100
19	294.0353	1200
20	293.0000	1300
21	291.9647	1400
22	291.0000	1400
23	290.1716	1350
24	289.5359	1300

References

Albu, M., Barnes, I., Becker, K. H., Patroescu-Klotz, I., Benter, T., and Mocanu, R.: FT-IR Product Study On The OH Radical Initiated Oxidation Of Dimethyl Sulfide: Temperature And O_2 Partial Pressure Dependence, in: Simulation and Assessment of Chemical Processes in a Multiphase Environment, edited by Barnes, I. and Kharytonov, M. M., pp. 501–513, Springer Science, Dortdrecht, https://doi.org/10.1007/978-1-4020-8846-9_41, 2008.

Atkinson, R., Baulch, D. L., Cox, R. A., Crowley, J. N., Hampson, R. F., Hynes, R. G., Jenkin, M. E., Rossi, M. J., and Troe, J.: Evaluated kinetic and photochemical data for atmospheric chemistry: Volume I - gas phase reactions of O_x, HO_x, NO_x and SO_x species, Atmos. Chem. Phys., 4, 1461–1738, https://doi.org/10.5194/acp-4-1461-2004, 2004.

Berndt, T., Scholz, W., Mentler, B., Fischer, L., Hoffmann, E. H., Tilgner, A., Hyttinen, N., Prisle, N. L., Hansel, A., and Herrmann, H.: Fast Peroxy Radical Isomerization and OH Recycling in the Reaction of OH Radicals with Dimethyl Sulfide, J. Phys. Chem. Lett., 10, 6478–6483, https://doi.org/10.1021/acs.jpclett.9b02567, 2019.

Berndt, T., Chen, J., Møller, K. H., Hyttinen, N., Prisle, N. L., Tilgner, A., Hoffmann, E. H., Herrmann, H., and Kjaergaard, H. G.: SO_2 formation and peroxy radical isomerization in the atmospheric reaction of OH radicals with dimethyl disulfide, Chem. Commun., 56, 13 634–13 637, https://doi.org/10.1039/D0CC05783E, 2020.

Burkholder, J. B., Sander, S. P., Abbatt, J. P. D., Barker, J. R., Cappa, C., Crounse, J. D., Dibble, T. S., Huie, R. E., Kolb, C. E., Kurylo, M. J., Orkin, V. L., Percival, C. J., Wilmouth, D. M., and Wine, P. H.: Chemical Kinetics and Photochemical Data for Use in Atmospheric Studies, Evaluation No. 19, Tech. rep., JPL Publication 19-5, Jet Propulsion Laboratory, Pasadena, http://jpldataeval.nasa.gov/, 2019.

Hoffmann, E. H., Tilgner, A., Schrödner, R., Bräuer, P., Wolke, R., and Herrmann, H.: An advanced modeling study on the impacts and atmospheric implications of multiphase dimethyl sulfide chemistry, Proc. Natl. Acad. Sci. U. S. A., 113, 11 776–11 781, https://doi.org/10.1073/pnas.1606320113, 2016.

Hynes, A. J. and Wine, P. H.: The atmospheric chemistry of dimethylsulfoxide (DMSO) kinetics and mechanism of the OH+DMSO reaction, J. Atmos. Chem., 24, 23–37, https://doi.org/10.1007/BF00053821, 1996.

Jernigan, C. M., Fite, C. H., Vereecken, L., Berkelhammer, M. B., Rollins, A. W., Rickly, P. S., Novelli, A., Taraborrelli, D., Holmes, C. D., and Bertram, T. H.: Efficient Production of Carbonyl Sulfide in the Low-NO_x Oxidation of Dimethyl Sulfide, Geophys. Res. Lett., 49, e2021GL096 838, https://doi.org/https://doi.org/10.1029/2021GL096838, 2022.

Kukui, A., Borissenko, D., Laverdet, G., and Le Bras, G.: Gas-Phase Reactions of OH Radicals with Dimethyl Sulfoxide and Methane Sulfinic Acid Using Turbulent Flow Reactor and Chemical Ionization Mass Spectrometry, J. Phys. Chem. A, 107, 5732–5742, https://doi.org/10.1021/jp0276911, 2003.

Lucas, D. D. and Prinn, R. G.: Mechanistic studies of dimethylsulfide oxidation products using an observationally constrained model, J. Geophys. Res.: Atmos., 107, ACH 12 1–26, https://doi.org/https://doi.org/10.1029/2001JD000843, 2002.

Sander, S. P., Abbatt, J., Barker, J. R., Burkholder, J. B., Friedl, R. R., Golden, D. M., Huie, R. E., Kolb, C. E., Kurylo, M. J., Moortgat, G. K., Orkin, V. L., and Wine, P. H.: Chemical Kinetics and Photochemical Data for Use in Atmospheric Studies, Evaluation No. 17, Tech. rep., JPL Publication 10-6, Jet Propulsion Laboratory, Pasadena, http://jpldataeval.nasa.gov/, 2011.

Shen, J., Scholz, W., He, X.-C., Zhou, P., Marie, G., Wang, M., Marten, R., Surdu, M., Rörup, B., Baalbaki, R., Amorim, A., Ataei, F., Bell, D. M., Bertozzi, B., Brasseur, Z., Caudillo, L., Chen, D., Chu, B., Dada, L., Duplissy, J., Finkenzeller, H., Granzin, M., Guida, R., Heinritzi, M., Hofbauer, V., Iyer, S., Kemppainen, D., Kong, W., Krechmer, J. E., Kürten, A., Lamkaddam, H., Lee, C. P., Lopez, B., Mahfouz, N. G. A., Manninen, H. E., Massabò, D., Mauldin, R. L., Mentler, B., Müller, T., Pfeifer, J., Philippov, M., Piedehierro,

A. A., Roldin, P., Schobesberger, S., Simon, M., Stolzenburg, D., Tham, Y. J., Tomé, A., Umo, N. S., Wang, D., Wang, Y., Weber, S. K., Welti, A., Wollesen de Jonge, R., Wu, Y., Zauner-Wieczorek, M., Zust, F., Baltensperger, U., Curtius, J., Flagan, R. C., Hansel, A., Möhler, O., Petäjä, T., Volkamer, R., Kulmala, M., Lehtipalo, K., Rissanen, M., Kirkby, J., El-Haddad, I., Bianchi, F., Sipilä, M., Donahue, N. M., and Worsnop, D. R.: High Gas-Phase Methanesulfonic Acid Production in the OH-Initiated Oxidation of Dimethyl Sulfide at Low Temperatures, Environ. Sci. Technol., 56, 13 931–13 944, https://doi.org/10.1021/acs.est.2c05154, 2022.

Veres, P. R., Neuman, J. A., Bertram, T. H., Assaf, E., Wolfe, G. M., Williamson, C. J., Weinzierl, B., Tilmes, S., Thompson, C. R., Thames, A. B., Schroder, J. C., Saiz-Lopez, A., Rollins, A. W., Roberts, J. M., Price, D., Peischl, J., Nault, B. A., Møller, K. H., Miller, D. O., Meinardi, S., Li, Q., Lamarque, J.-F., Kupc, A., Kjaergaard, H. G., Kinnison, D., Jimenez, J. L., Jernigan, C. M., Hornbrook, R. S., Hills, A., Dollner, M., Day, D. A., Cuevas, C. A., Campuzano-Jost, P., Burkholder, J., Bui, T. P., Brune, W. H., Brown, S. S., Brock, C. A., Bourgeois, I., Blake, D. R., Apel, E. C., and Ryerson, T. B.: Global airborne sampling reveals a previously unobserved dimethyl sulfide oxidation mechanism in the marine atmosphere, Proc. Natl. Acad. Sci. U. S. A., 117, 4505–4510, https://doi.org/10.1073/pnas.1919344117, 2020.

Vermeuel, M. P., Novak, G. A., Jernigan, C. M., and Bertram, T. H.: Diel Profile of Hydroperoxymethyl Thioformate: Evidence for Surface Deposition and Multiphase Chemistry, Environ. Sci. Technol., 54, 12 521–12 529, https://doi.org/10.1021/acs.est.0c04323, 2020.

Wu, R., Wang, S., and Wang, L.: New Mechanism for the Atmospheric Oxidation of Dimethyl Sulfide. The Importance of Intramolecular Hydrogen Shift in a CH_3SCH_2OO Radical, J. Phys. Chem. A, 119, 112–117, https://doi.org/10.1021/jp511616j, 2015.

Ye, Q., Goss, M. B., Isaacman-VanWertz, G., Zaytsev, A., Massoli, P., Lim, C., Croteau, P., Canagaratna, M., Knopf, D. A., Keutsch, F. N., Heald, C. L., and Kroll, J. H.: Organic Sulfur Products and Peroxy Radical Isomerization in the OH Oxidation of Dimethyl Sulfide, ACS Earth Space Chem., 5, 2013–2020, https://doi.org/10.1021/acsearthspacechem.1c00108, 2021.

Ye, Q., Goss, M. B., Krechmer, J. E., Majluf, F., Zaytsev, A., Li, Y., Roscioli, J. R., Canagaratna, M., Keutsch, F. N., Heald, C. L., and Kroll, J. H.: Product distribution, kinetics, and aerosol formation from the OH oxidation of dimethyl sulfide under different RO_2 regimes, Atmos. Chem. Phys., 22, 16 003–16 015, https://doi.org/10.5194/acp-22-16003-2022, 2022.

Yin, F., Grosjean, D., and Seinfield, J. H.: Photooxidation of dimethyl sulfide and dimethyl disulfide. I: Mechanism development, J. Atmos. Chem., 11, 309–364, https://doi.org/https://doi.org/10.1007/BF00053780, 1990.